


Fabrication of Optimized Superconducting Phase Inverters Based on Superconductor–Ferromagnet–Superconductor π -Junctions

V. V. Bolginov^{1,2}  · A. N. Rossolenko¹ ·
A. B. Shkarin^{1,4} · V. A. Oboznov¹ ·
V. V. Ryazanov^{1,2,3}

Received: 19 October 2017 / Accepted: 14 December 2017 / Published online: 28 December 2017
© Springer Science+Business Media, LLC, part of Springer Nature 2017

Abstract We have implemented a trilayer technological approach to fabricate Nb–Cu_{0.47}Ni_{0.53}–Nb superconducting phase inverters (π -junctions) with enhanced critical current. Within this technique, all three layers of the superconductor–ferromagnet–superconductor junction deposited in a single vacuum cycle that have allowed us to obtain π -junctions with critical current density up to 20 kA/cm². The value achieved is a factor of 10 higher than for the step-by-step method used in earlier works. Our additional experiments have shown that this difference is related to a bilayered CuNi/Cu barrier used in the case of the step-by-step technique and interlayer diffusion at the CuNi/Cu interface. We show that the interlayer diffusion can be utilized for fine tuning of the 0– π transition temperature of already fabricated junctions. The results obtained open new opportunities for the CuNi-based phase inverters in digital and quantum Josephson electronics.

Keywords Magnetic Josephson junctions · π -Junctions · Phase invertors · Thin-film multilayered technology

✉ V. V. Bolginov
bolg@issp.ac.ru

¹ Institute of Solid State Physics, Russian Academy of Sciences, 2 Academician Ossipyan Str., Chernogolovka, Moscow District, Russia 142432

² National University of Science and Technology MISiS, Moscow, Russia 119991

³ Faculty of Physics, National Research University Higher School of Economics, 21/4 Staraya Basmannaya Str., Moscow, Russia 105066

⁴ Present Address: Max Planck Institute for the Science of Light, Staudtstr. 2, 91058 Erlangen, Germany

1 Introduction

According to numerous forecasts, it is impossible to keep increasing integration of elements and energy efficiency in semiconducting electronics at the present rate (see, for example, [1]). A further development has to use new conceptual non-dissipative solutions such as superconducting computing. Rapid single flux quantum (RSFQ) digital superconducting circuits demonstrate very high clock speed and low power dissipation [2–5]. These important advantages together with low dispersion interconnect provide good prospects for a wide variety of applications ranging from digital radio frequency receivers [6,7] to high-end computing [8]. Further development of superconducting digital and quantum logics may be augmented by the use of superconductor–ferromagnet–superconductor (SFS) Josephson junctions [9–12]. For example, implementation of fundamentally new Josephson switches using ferromagnetic barrier remagnetization by magnetic pulses [13,14] can be important for realization of a quick Josephson memory [1,15–17]. Another promising area of application of SFS junctions is using them as superconducting phase inverters (Josephson π -junctions) [18–20] to reduce RSFQ digital logic cell sizes [10–12] and to increase the coherence time of superconducting quantum logic elements (superconducting qubits) [9,11,21]. The π -state, which is characterized by an inverted current–phase relation $I = -I_c \sin(\phi)$, originates from oscillations of the superconducting order parameter in a ferromagnet close to FS-interface in a Josephson SFS junction [18,22,23]. Incorporation of a π -junction in a superconducting circuit is equivalent to applying half of a magnetic flux quantum [24], which allows to realize new algorithms of RSFQ logic functionality [10] and to switch superconducting qubits to working regime without applying a magnetic field [21]. The main requirement for this passive π -shifter (or phase inverter) is a much larger critical current compared to the other (“dynamical”) Josephson junctions in a closed cell of the superconducting circuit. This guarantees that the π -junction behaves as a static source of π phase shift and does not disturb the functioning of other elements.

Presently very promising candidates for implementing “ π -RSFQ circuits” are SFS junctions based on a weak-ferromagnetic CuNi barrier. Copper and nickel are cheap and form a wide set of weak magnetic alloys at nickel concentrations in the range of 50–60 at.%. In addition, the fabrication of Nb–CuNi–Nb junctions is compatible with present Nb–AlO_x–Nb technology of RSFQ circuits. In [20] we have demonstrated Nb–Cu_{0.47}Ni_{0.53}–Nb π -junctions with a critical current density up to 1 kA/cm² which in principle is high enough to use them in superconducting digital and quantum cells [11,12]. It is important that Cu_{0.47}Ni_{0.53} layers possess a fine domain structure with an out-of-plane magnetic anisotropy [25], and the virgin domain structure is stable, i.e., it does not change for working in-plane magnetic fields which are much smaller than the coercive field ~ 200 Oe [26]. This ensures that the initial state of the ferromagnetic Josephson barrier has zero net macroscopic magnetization, and results in stable critical current and π -shift during the SFS phase inverter operation. The relatively small exchange field ($T_{\text{Curie}} \approx 60$ K) provides a large decay length and spatial oscillation period of the induced superconducting order parameter, that improves the reproducibility of the critical current density and the discrimination between conventional (“0”-) and π -states. This keeps the relevance of the CuNi alloy use for the phase

inverter although a substantial progress had also been achieved with the use of strong single-element ferromagnets with about 1 nm thick interlayer [27,28].

Despite the success reported in [11,12,20], the task to increase the critical current density of Nb–CuNi–Nb π -junctions remains essential. In this work we consider the technological aspects of the task. Specifically, we compare two different technologies of Nb–Cu_{0.47}Ni_{0.53}–Nb junction fabrication. The first one is a step-by-step technique used in the pioneer works [19,20,29]. The defining feature of this technology is that each of the three layers is deposited and formed in an individual technological cycle. This technique is simple, and it imposes minimal requirements on fabrication equipment; however, special technological methods must be used to ensure good transparency of the interlayer interface and to preserve the properties of the ferromagnetic layer. The other (trilayer) technique requires deposition of the ferromagnetic and both superconducting layers of the final SFS structure in a single vacuum cycle at the beginning of the technology process. This technology is generally more complicated, but it provides the best possible transparency of SF-interfaces, resulting in a larger critical current density. At the beginning of our work the improvement of the interface transparency looked as the only way to increase the critical current of CuNi-based π -junctions. But in the course of the work, we have revealed one more advantage of the trilayer approach as compared to the step-by-step one which ensured the increase in the π -state critical current density by an order of magnitude.

2 Fabrication Techniques

The step-by-step approach (see Fig. 1a–d starts with the magnetron deposition of the bottom Nb layer (typically, of 120 nm thick) on a Si substrate coated by a thin AlO_x layer. The bottom superconducting electrode is then formed (Fig. 1a) using photolithography and wet etching in a mixture of HF and HNO₃ acids. This electrode includes bottom bias lead and contact pads for a measurement setup. The second step is the deposition of CuNi/Cu bilayered barrier by the RF-sputtering, and its subsequent patterning by means of photolithography and wet etching in diluted FeCl₃ (Fig. 1b). The bilayer is shaped as a square with a side which is 10–15 μ m larger than the size of the designed Josephson junction. The need for the additional Cu layer (initially

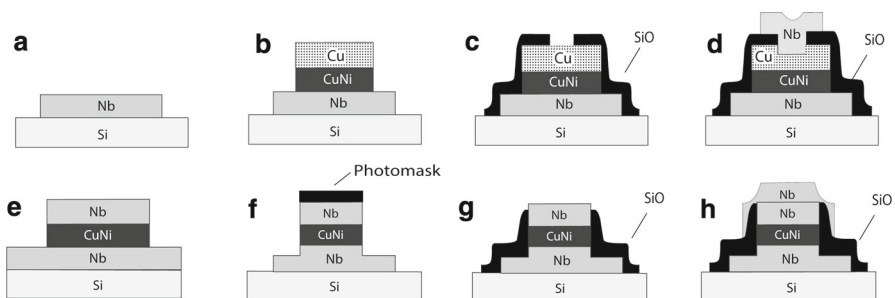


Fig. 1 Basic steps of the SFS junction fabrication using the step-by-step technique (top row) and the trilayer technique (bottom row)

with a thickness of 50 nm) is explained below. During the third step an insulating SiO layer (typically, of 170 nm thick) is deposited by thermal evaporation. The subsequent lift-off process “opens a window” in the insulator to the CuNi/Cu layer (Fig. 1c) and thus defines the final dimensions of the Josephson junction. The last step is the creation of the top superconducting Nb wiring (typically, of 240 nm thick) using magnetron sputtering and a lift-off process (Fig. 1d). This layer serves as a top electrode and completes the bias bus for a 4-point measurement scheme.

The key feature of this technique is that sputtering of each layer happens in a separate vacuum cycle. To ensure good interface quality, an ion etching of the structure is carried out before each layer deposition. This procedure is needed to remove oxide layers and organic residues (resist, developer, solvents, etc.) from the surface of previously deposited and formed layers. However, this straightforward way to clean up the surface leads to problems when applied to the ferromagnetic barrier layer. Since SFS junction critical current depends strongly on the CuNi layer thickness and composition, the direct cleaning of the ferromagnetic layer is undesirable. Indeed, the small (1.3 nm [20]) decay length of the superconducting order parameter in the Josephson $\text{Cu}_{0.47}\text{Ni}_{0.53}$ barrier imposes strict requirements on the reproducibility of the etching process and the invariability of the ferromagnet chemical composition. For this reason, we use an additional thin “protective” copper layer sputtered right after CuNi deposition in the same vacuum cycle. In [19] the initial thickness of the copper layer was 50 nm, while its final thickness after argon cleaning was 20 nm. In [20] several samples were fabricated with thinner Cu layers: 20 nm for the initial thickness and 10 nm for the final one. This allowed us to obtain SFS junctions with more uniform barriers, and with that demonstrate transitions to the π -state and back to the conventional “0”-state by changing temperature and barrier thickness. In our previous works we assumed that the effect of the thin Cu layer is reduced to an additional weak decay of superconductivity, which could be neglected since the superconducting coherence length in copper $\xi_{\text{Cu}} \approx 57 \text{ nm}$,¹ is much larger than the CuNi decay length, and the Cu layer thickness is smaller than ξ_{Cu} . However, in this work we have found a more significant effect of the additional Cu layer, which we will discuss in the next section.

The trilayer technique is a commonly used method to prepare high-quality multilayered Josephson junctions. Its basics were worked out about 30 years ago while developing the technology for fabrication of Nb– AlO_x –Nb tunnel junctions [31]. The key point of this method is the deposition of both superconducting layers and the Josephson interlayer in a single vacuum cycle with subsequent processing to form the junction area, create insulation, superconducting leads and contact pads. Several groups already use this method to fabricate magnetic Josephson junctions (see [27, 32–37] for example). We also had begun to use this approach as it was described in [13, 14]. Below we present the so-called self-aligned technological process which we use to fabricate junctions with areas down to $2 \times 2 \mu\text{m}^2$ (see Fig. 1e–h).

¹ For the Cu layer in the dirty limit approximation, the coherence length is $\xi_{\text{Cu}} = (\hbar D / 2\pi kT)^{1/2}$, where $D = \frac{1}{3} l v_F$ is the diffusion coefficient, l is the mean free path and $v_F = 1.57 \times 10^8 \text{ cm/s}$ is the Fermi velocity. To estimate the mean free path, we have used $\rho \cdot l = 6.49 \text{ p}\Omega \text{ cm}$ relation [30], where $\rho \approx 3 \mu\Omega \text{ cm}$ according to the resistivity measurements for our copper films.

The self-aligned method starts with a Nb–CuNi–Nb trilayer fabrication on a Si substrate coated by a thin AlO_x layer. As in the previous case, we use the magnetron sputtering for Nb layers and the RF-sputtering to deposit CuNi interlayer. Thicknesses of the bottom and the top Nb layers are equal to 100 and 60 nm respectively. After that we use photolithography and Ar plasma etching to form the top Nb/CuNi bilayer in the shape of the future bottom Nb electrode of the structure (see Fig. 1e). During the next stage, we make a photoresistive mask defining the Josephson junction shape and then expose the substrate with our structure to another cycle of argon etching. Note that in this process the etching of the top bilayer through the mask forms the Josephson junction itself, while the etching of the niobium outside the bilayer simultaneously defines the bottom Nb electrode. In a way, the top Nb/CuNi bilayer serves as a protective mask for the bottom Nb layer at this stage. Thus, at the end of this stage we have formed both the lower superconducting electrode, including a bias bus and contact pads, and the square Nb/CuNi “mesa” of the desirable size (Fig. 1f). It is important that the photoresistive mask is retained after the process is completed. The fourth stage consists of the thermal evaporation of a SiO insulation layer on the structure with the preserved photoresistive mask, followed by a lift-off process (Fig. 1g). This process is called “self-aligned” because the same photoresistive mask simultaneously defines the junction shape and the window in the insulation layer.² The self-aligned method is completed by creating a wiring layer using the Nb magnetron sputtering and the lift-off process (Fig. 1h). It is important to note that the trilayer technology does not require a protective Cu layer, because the CuNi interlayer is immediately covered by the top Nb layer in the same vacuum cycle.

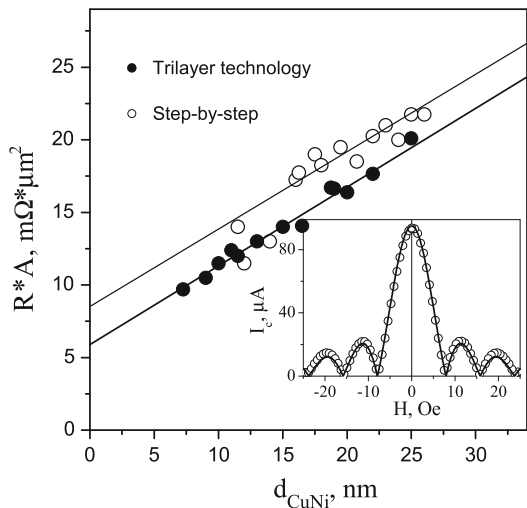
The main requirement for high-quality Josephson junctions is a uniform critical current density distribution along the junction. This is verified by measuring the dependence of the critical current vs. in-plane magnetic field, which should exhibit a well-known sinc (“Fraunhofer”) dependence. All junctions presented below satisfied this condition (see inset in Fig. 2), which allowed us to easily extract their critical current densities j_c . The junctions have a square shape with a size a ranging from 2 to 80 μm to fulfill the small junction limit ($a < 4\lambda_J$, where λ_J is the Josephson penetration length) for the smallest barrier thicknesses and to obtain an observable critical current for the largest ones. Experiments were carried out in a He-4 cryostat equipped with a superconducting solenoid creating a magnetic field parallel to the Si substrate plane. The junction characteristic voltage $I_c R_N$ varied approximately from 1 μV down to 10 pV, which forced us to use a SQUID-picovoltmeter for $I-V$ and $I_c(H)$ measurements. To ensure a small contact resistance (on the order of 1 $\mu\Omega$) between the junction and the SQUID-picovoltmeter circuit, we connected them using indium applied with an ultrasonic soldering iron. The measurement procedure was the same as in our previous works [19,20].

² If a special photoresistive mask is used to form the isolation, the “window” in the insulation layer has to be substantially less than the mesa size to ensure a good alignment and covering of the mesa edges. The corresponding picture is given, for example, in our work [13].

3 Experimental Results

The main goal of using the trilayer technology is to increase the interface transparency that should lead to an increase in the critical current density of the SFS junctions. To evaluate this effect, we had measured the dependence of the junction resistance on the CuNi thickness for the trilayer technique and compared it with the dependence obtained earlier for the step-by-step technique [20]. To extract the junction resistance values R , we fitted experimental IV -curves by the RSJ model relationship $V = R\sqrt{I^2 - I_c^2}$ using R as a fitting parameter. Figure 2 shows the resistance per unit junction area, $R \cdot A$, as a function of CuNi layer thickness. One can see that experimental data for both technologies can be approximated by a simple formula $R \cdot A = 2R_b A + \rho d$ where R_b is the SF interface resistance, $\rho = 54.2 \mu\Omega \text{ cm}$ is CuNi resistivity and A is the junction area. For the trilayer technique we can estimate $R_b \cdot A \approx 2.9 \text{ m}\Omega \mu\text{m}^2$, while for the step-by-step technique this parameter is about $4.2 \text{ m}\Omega \mu\text{m}^2$. One can see that the interface resistance for the step-by-step technique is indeed higher, but not dramatically: only by about 45%. Quantitatively the interface transparency in SFS junctions can also be characterized by a dimensionless parameter $\gamma_b = R_b A / \rho \xi_F$ [20,38], where $\xi_F = \sqrt{\hbar D / 2\pi k_B T_c}$, D is the electron diffusion coefficient for the ferromagnetic interlayer, and $T_c = 8.5 \text{ K}$ is the critical temperature for our Nb superconducting electrodes. Using the CuNi resistivity value obtained above and the relation for “dirty” copper $\rho_{\text{Cu}} \cdot l_{\text{Cu}} = 6.49 \text{ p}\Omega \text{ cm}^2$ [30], we can estimate the electron mean free path l for $\text{Cu}_{0.47}\text{Ni}_{0.53}$ as 1.2 nm and $D = \frac{1}{3}lv_F$ as $6.28 \text{ cm}^2/\text{s}$ (where $v_F = 1.57 \times 10^8 \text{ cm/s}$ is the electron Fermi velocity in copper) and also calculate values of $\xi_F = 9.5 \text{ nm}$ and γ_b equal to 0.57 and 0.82 for the trilayer and the step-by-step techniques respectively. For both processes γ_b values are less than unity which indicates high interface quality. It means that the argon etching really removes majority of the surface contamination in the process of the step-by-step technique.

Fig. 2 Junction resistance as a function of CuNi layer thickness for the trilayer technique (solid circles) and for the step-by-step technique (open circles). The inset shows a typical dependence of the critical current on the in-plane magnetic field for one of the Josephson junction fabricated using the trilayer technique. The solid line in the inset shows the fit by the Fraunhofer pattern



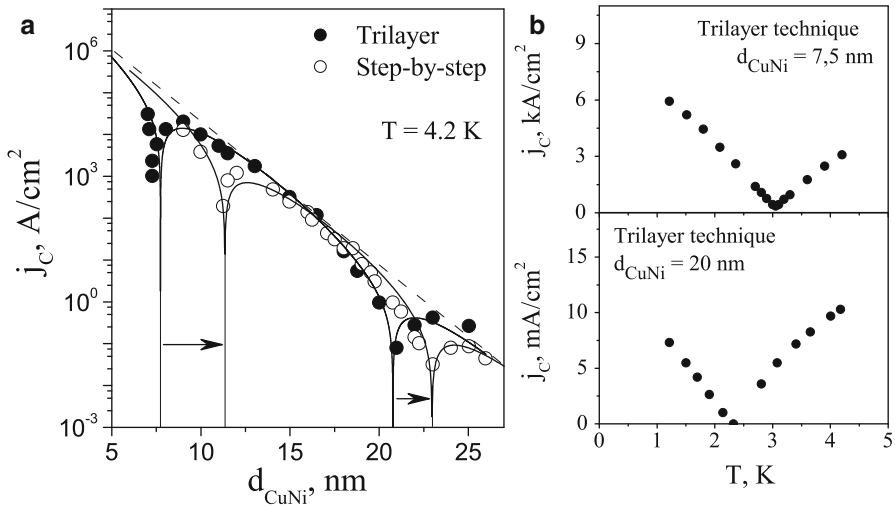


Fig. 3 **a** Critical current density as a function of CuNi layer thickness for the two different technologies. Solid lines represent fits by the simple formulas (1, 2), and the dashed line shows a common exponentially decay envelope described in the text. Open circles show the step-by-step technique data from [20], while the solid circles show the trilayer technique data obtained in the present work. **b** Reentrant temperature dependencies of the critical current density for samples with d_{CuNi} of 7 nm (top) and 20 nm (bottom) fabricated using the trilayer technique. These thicknesses correspond to deep dips ($0-\pi$ transitions) in (a)

Figure 3a presents the junction critical current density j_c as a function of CuNi layer thickness d_{CuNi} for the step-by-step technique (“open” data set), as well our new data obtained for the junctions fabricated by means of the trilayer technique (“solid” data set). Both $j_c(d_{\text{CuNi}})$ dependencies demonstrate two nodes separating ranges of the conventional (“0”-) and the π -states. One can see that both data sets have the same envelope described by an exponential decay $j_0 \exp(-d_{\text{CuNi}}/\xi_{\text{F1}})$ with the same characteristic length $\xi_{\text{F1}} \approx 1.3$ nm and the pre-exponential factor $j_0 = 6 \times 10^7$ A/cm². This shows that the increase in the interface transparency obtained for the trilayer technique does not lead to a significant increase in the j_0 value.

For barrier thicknesses close to the nodal values, we observe reentrant dependencies $j_c(T)$ (Fig. 3b), which arise due to temperature-dependent quasiparticle processes in SFS junctions with spin-flip scattering in the barrier (see [20]). The sharp cusps in these curves are the best indicator of the transitions between 0- and π -states, demonstrating that these transitions occur for CuNi thicknesses around 7 and 20 nm in the junctions fabricated by means of the trilayer technique. At the same time, the step-by-step technique demonstrates transition thicknesses which are 3–4 nm larger, while the overall exponential envelope $j_0 \exp(-d_{\text{CuNi}}/\xi_{\text{F1}})$ remains the same. This increase in the transition thicknesses is quite large as compared to the exponential decay length of 1.3 nm that provides a huge increase in the π -junction critical currents: The maximal critical current in the π -state obtained for the trilayer technique is 10–20 kA/cm², which is one order of magnitude larger than that for the step-by-step technology. Thus, the main goal of our work had been achieved, and below we will give an explanation of the effect observed.

To analyze the results obtained, we have fitted both experimental curves $j_c(d_{\text{CuNi}})$ in Fig. 3a by the following simple formula [20,23]:

$$j_c = j_0 \exp\left(-\frac{d_{\text{CuNi}}}{\xi_{\text{F1}}}\right) \left(\cos\left(\frac{d_{\text{CuNi}}}{\xi_{\text{F2}}}\right) + \frac{\xi_{\text{F1}}}{\xi_{\text{F2}}} \sin\left(\frac{d_{\text{CuNi}}}{\xi_{\text{F2}}}\right) \right) \quad (1)$$

Here $\xi_{\text{F1,2}}$ are the real (related to decay) and the imaginary (related to oscillations) parts of the complex superconducting coherence length in a ferromagnet. It was shown in [20] that for the step-by-step technique we had to introduce one more fitting parameter: a thickness d_0 of so-called dead layer representing a non-magnetic part of the CuNi layer which does not contribute to the “sign-reversal superconductivity”. We believe that the origin of the dead layer is related to the bilayered CuNi/Cu composition of Josephson barriers which we use in the case of the step-by-step technology. Indeed, nickel atoms can penetrate easily from the CuNi layer into the copper layer due to the diffusion process. The diffusion takes place at any temperature, but it is accelerated if a sample is heated. The heating occurs, for example, during the photolithography process (90–100°C) or during the sample bonding using an ultrasound soldering iron. Because of the withdrawal of nickel near the CuNi/Cu interface, the nickel content falls below its critical value ($\approx 44\%$) for the ferromagnetism onset in CuNi, and a non-magnetic dead layer mentioned above arises (see Fig. 4a). Formally in this case one has to replace d_{CuNi} in the oscillating part of (1) by $d_{\text{CuNi}} - d_0$ where $d_0 \approx 4$ nm is the dead layer thickness obtained from the fit to the open points in Fig. 3a.

The decay of superconductivity in a CuNi/Cu barrier is defined by three sublayers: the ferromagnetic CuNi layer, a pure part of the protective Cu layer and a so-called diffusive layer of a thickness d_d composed of the dead layer and a Ni-contaminated part of the Cu layer (see Fig. 4a). Compared to the trilayer technique (where only the CuNi layer is present), the decay factor due to ferromagnetic part is $\exp(d_0/\xi_{\text{F1}})$ larger. This increase is compensated by a decay factor due to diffusive layer $\exp(-d_d/\xi_d)$, and some additional decay by a factor of ~ 0.67 is introduced by the non-contaminated part of the protective copper layer. The effective coherence length ξ_d in the diffusive layer is larger than ξ_{F1} due to the absence of exchange interaction, but the thickness d_d is also larger than d_0 , which can compensate for the increase in ξ_d . Invariability of the exponential envelope $j_0 \exp(-d_{\text{CuNi}}/\xi_{\text{F1}})$ in Fig. 3a suggests that these changes approximately balance each other out, so the $j_c(d_{\text{CuNi}})$ dependence could be approximated by the following expression in the case of the step-by-step technique:

$$j_c = j_0 \exp\left(-\frac{d_{\text{CuNi}}}{\xi_{\text{F1}}}\right) \left(\cos\left(\frac{d_{\text{CuNi}} - d_0}{\xi_{\text{F2}}}\right) + \frac{\xi_{\text{F1}}}{\xi_{\text{F2}}} \sin\left(\frac{d_{\text{CuNi}} - d_0}{\xi_{\text{F2}}}\right) \right) \quad (2)$$

Thus, the nickel diffusion from the CuNi layer to the Cu layer simply shifts the $0-\pi$ transition points to larger CuNi thicknesses and does not affect substantially the exponentially decaying envelope. At the moment it is difficult to say whether this statement is fundamental or it is applicable only for the particular experiment under discussion. One way or another, the interlayer diffusion that occurred during the step-by-step fabrication and wiring of our samples was very reproducible, which allowed us to obtain a sufficiently smooth $j_c(d_{\text{CuNi}})$ curve and to compare it well with theoretical models [20,23].

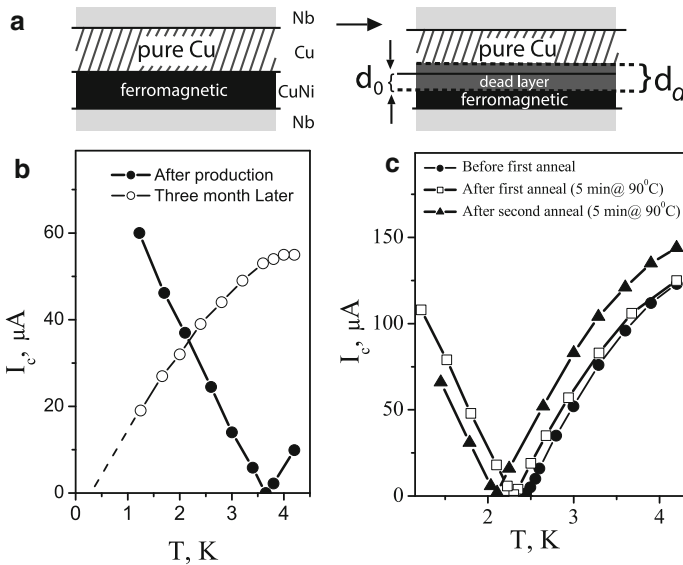


Fig. 4 **a** Schematic illustration of changes in CuNi/Cu bilayer structure due to interlayer diffusion process. Here d_0 marks the thickness of an effective “dead layer” in the ferromagnetic barrier, d_d is a total thickness of the paramagnetic $\text{Cu}_{1-x}\text{Ni}_x$ layer (a diffusive layer) with the Ni concentration $x < 44\%$. **b** A temperature dependence of the critical current for S–N/F/N–S junction with two “protective” Cu layers. Solid circles show the measurement results right after the sample preparation, while the open circles show the same dependence for the same device measured 3 month later. The $0-\pi$ transition temperature decreased due to the Ni diffusion from the CuNi interlayer into the two Cu layers. **c** Reentrant temperature dependence for S–F/N–S junction (Nb–CuNi/Cu–Nb) just after fabrication and after two low-temperature annealings illustrating the possibility to adjust $0-\pi$ transition temperature by means of stimulated interlayer diffusion

To test the diffusion hypothesis in more detail, we have fabricated a special SFS junction containing CuNi barrier sandwiched between two copper layers. The CuNi thickness was chosen to be at the $0-\pi$ transition point and to demonstrate the reentrant $j_c(T)$ dependence similar to the ones shown in Fig. 3b. As noted above, insertion of 20 nm Cu layer in the course of the step-by-step technique increases this transition thickness by about 4 nm compared to the trilayer technique: from 7 to 11 nm (see Figure 3(a) and Figure 2 in [20]). Therefore, for the Nb–Cu/Cu_{0.47}Ni_{0.53}/Cu–Nb junction with two copper layers we can expect the double increase of the transition thickness, resulting in the $0-\pi$ transition at $d_{\text{CuNi}} \approx 7 \text{ nm} + 2 \times 4 \text{ nm} = 15 \text{ nm}$. Indeed, Josephson S–N/F/N–S junction with CuNi interlayer of this thickness and two Cu layers fabricated using the step-by-step technique had demonstrated the reentrant temperature dependence of the critical current (solid points in Fig. 4b), which confirmed our hypothesis about the origin of the dead layer in the step-by-step fabricated SFS junctions.

4 Discussion

We have shown that the interlayer diffusion is an important factor that must be taken into account when fabricating multilayer hybrid structures. Furthermore, its presence

allows us to explain some previously observed peculiar properties of SFS junctions with a protective Cu layer. While repeated measurements of Nb–CuNi/Cu–Nb junctions during the past decade [19,20] we had noticed that they are subjected to aging. To detect this effect, it is best to measure the reentrant temperature dependence of the critical current and track the $0-\pi$ transition temperature T_π . It was shown in [19,20] that this value is very sensitive to the F-layer thickness: Increasing d_{CuNi} by 1 nm increases T_π by about 3 K. We have observed that T_π decreases with time, which indicates a decrease in the effective F-layer thickness. This process is especially noticeable in SFS junctions with a trilayer Cu/CuNi/Cu barrier. One can see in Fig. 4b that the $0-\pi$ transition temperature had dropped from 3.5 K to below 1 K in 3 months, which corresponds to 1 nm change in the effective F-layer thickness. We can readily attribute this effect to slow Ni diffusion at room temperature. For a bilayered CuNi/Cu barrier this process is weaker, as it has only one CuNi/Cu interface. Finally, for trilayer SFS samples with a monolayer barrier we did not observe any changes of T_π with time or during low-temperature annealing at temperatures 90–100°C typical for photolithography process.

In our earlier works some other manifestations of the interlayer diffusion have also been reported. For example, a dead layer formation has been reported in [39] devoted to multilayer SIFS junctions that simultaneously contain a tunnel AlO_x barrier and a ferromagnetic Ni barrier. Although all layers of this SIFS structure were deposited in a single vacuum cycle, the tunnel and the ferromagnetic layers were separated by a thin copper layer, and the interlayer diffusion could be substantial. A finer effect was reported in [40] in which Nb–CuNi/Cu–Nb junctions were studied in the close proximity to the $0-\pi$ transition point. Since the samples were fabricated using the step-by-step technique, the junction area was defined by a window in an insulation layer. Figure 1d shows that the thickness of the protective copper layer is nonuniform close to the edges of the window, so one could expect a step in the effective ferromagnetic barrier thickness. Indeed, in the vicinity of the $0-\pi$ transition thickness we had observed the junction separation into 0 - and π -state regions, which resulted in non-trivial interference patterns and half-integer Shapiro steps. This effect is very subtle and is related to the narrow edge region with a submicron width near the window boundary, while the decrease in the effective barrier thickness was no more than 1 nm. To eliminate this effect we had decreased the initial copper layer thickness as well as the step height arising due to etching (as was mentioned in Sect. 2). This had allowed us to obtain Nb–CuNi/Cu–Nb junctions with a uniform distribution of the critical current, which demonstrated a typical (Fraunhofer) dependence of the critical current on the in-plane magnetic field as well as sharp temperature transitions to the π -state and back to the conventional 0 -state [20].

All of the above shows that the trilayer technology is more suitable for fabrication of stable and uniform π -junctions for use as phase inverters in superconducting electronics. Our ongoing investigations also show that the use of the trilayer technique is important for detection of a second Fourier component of the Josephson current-phase relation at the $0-\pi$ transition because it occurs at a lower F-layer thickness that allows to observe an unusual π -periodic current-phase relation [41,42] at the transition point. Nevertheless, the step-by-step technology may also be useful as it allows to tune the effective ferromagnetic barrier thickness of already prepared samples. Indeed, a low-temperature annealing activates the interlayer diffusion process that can result in a

decrease in the effective CuNi thickness. This process can be useful if one needs to precisely engineer the $0-\pi$ transition temperature, T_π , to observe phenomena close to the transition. Since T_π depends on the F-layer thickness very sharply (about 3 K per 1 nm), it is difficult to set a desired T_π just by varying the ferromagnetic layer thickness. On the other hand, low-temperature annealing allows us to adjust the $0-\pi$ transition point with 0.2 K accuracy (see Fig. 4c). It means that we can tune the effective barrier layer thickness with an ultimate precision of about 0.05 nm.

5 Summary

In this work we report on the fabrication of Nb–Cu_{0.47}Ni_{0.53}–Nb π -junctions with critical current density j_c up to 20 kA/cm². This is about 10 times larger than our previously obtained results and opens new possibilities for use of the phase inverters in superconducting digital and quantum circuits. This increase is achieved due to using of a more modern “trilayer” fabrication process which starts from deposition of both superconducting banks and ferromagnetic barrier in a single vacuum cycle. In our previous works we used a simpler step-by-step approach in which each layer was deposited and processed individually. In the latter case we have obtained the same exponentially decaying envelope of the nonmonotonic j_c on the CuNi thickness dependence, but $0-\pi$ transitions took place at larger thicknesses. We show that this difference is related to the CuNi/Cu bilayer structure of the ferromagnetic barrier used in the step-by-step fabrication process. An additional protective Cu layer needed in this technique does not affect substantially the critical current by itself, but it causes a change of the CuNi layer composition close to the interface due to the interlayer diffusion. This decreases the effective ferromagnetic layer thickness and creates a non-ferromagnetic “dead layer” observed in previous works (see, for example [20]). The interlayer diffusion decreases the maximal critical current density in the π -state but, on the other hand, allows to tune the effective ferromagnet barrier thickness in already prepared samples by means of a low-temperature annealing.

Acknowledgements Authors thank N.S. Stepanov, V.N. Shilov, A. Puchkov and D.S. Sobanin for their assistance in sample fabrication and performing measurements, S.M. Frolov for helpful discussions and also A.V. Nadochenko and V.O. Shkolnikov for their participation in the manuscript preparation. This work was supported by Russian Foundation for Basic Research grant #17-02-01270 and the Ministry for Education and Science of Russian Federation in the framework of Increase Competitiveness Program of NUST (MISiS) under contract no. K2-2014-025.

Compliance with ethical standards

Conflict of interest The authors declare that they have no conflict of interest.

Data Availability All substantial data generated and analyzed during this study are included in this published article.

References

1. D.S. Holmes, A.L. Ripple, M.A. Manheimer, Energy-efficient superconducting computing-power budgets and requirements. *IEEE Trans. Appl. Supercond.* **23**, 1701610 (2013)

2. K. Likharev, V. Semenov, RSFQ logic/memory family: a new Josephson-junction technology for sub-terahertz clock-frequency digital systems. *IEEE Trans. Appl. Supercond.* **1**, 3–28 (1991)
3. W. Chen, A.V. Rylyakov, V. Patel, J.E. Lukens, K.K. Likharev, Superconductor digital frequency divider operating up to 750 GHz. *Appl. Phys. Lett.* **73**, 2817–2819 (1998)
4. M. Tanaka, H. Akaike, A. Fujimaki, Y. Yamanashi, N. Yoshikawa, S. Nagasawa, K. Takagi, N. Takagi, 100-GHz single flux quantum bit-serial adder based on 10- kA/cm² niobium process. *IEEE Trans. Appl. Supercond.* **21**, 792–796 (2011)
5. T.V. Filippov, A. Sahu, A.F. Kirichenko, I.V. Vernik, M. Dorojevets, C.L. Ayala, O.A. Mukhanov, 20 GHz operation of an asynchronous wave-pipelined RSFQ arithmetic-logic unit. *Phys. Proc.* **36**, 59–65 (2012)
6. O.A. Mukhanov, D. Kirichenko, I.V. Vernik et al., Superconductor digital-RF receiver systems. *IEICE Trans. Electron.* **21**(E91-C), 306–17 (2008).
7. I.V. Vernik, D.E. Kirichenko, V.V. Dotsenko, R. Miller, R.J. Webber, P. Shevchenko, A. Talalaevskii, D. Gupta, O.A. Mukhanov, Cryocooled wideband digital channelizing RF receiver based on low-pass ADC. *Supercond. Sci. Technol.* **20**, S323–7 (2007)
8. A. Silver, A. Kleinsasser, G. Kerber, Q. Herr, M. Dorojevets, P. Bunyk, L. Abelson, Development of superconductor electronics technology for high-end computing. *Supercond. Sci. Technol.* **16**, 1368–1374 (2003)
9. G. Blatter, V.B. Geshkenbein, L. Ioffe, Design aspects of superconducting-phase quantum bits. *Phys. Rev. B* **63**, 174511 (2001)
10. A.V. Ustinov, V.K. Kaplunenko, Rapid single-flux quantum logic using π -shifters. *J. Appl. Phys.* **94**, 5405 (2003)
11. A.K. Feofanov et al., Implementation of superconductor/ferromagnet/superconductor π -shifters in superconducting digital and quantum circuits. *Nat. Phys.* **6**, 593 (2010)
12. M.I. Khabipov, D.V. Balashov, F. Maibaum, A.B. Zorin, V.A. Oboznov, V.V. Bolginov, A.N. Rossolenko, V.V. Ryazanov, A single flux quantum circuit with a ferromagnet-based Josephson π -junction. *Supercond. Sci. Technol.* **23**, 045032 (2010)
13. V.V. Bol'ginov, V.S. Stolyarov, D.S. Sobanin, A.L. Karpovich, V.V. Ryazanov, Magnetic switches based on Nb–PdFe–Nb Josephson junctions with a magnetically soft ferromagnetic interlayer. *JETP Lett.* **95**, 366 (2012)
14. T.I. Larkin, V.V. Bol'ginov, V.S. Stolyarov, V.V. Ryazanov, I.V. Vernik, S.K. Tolpygo, O.A. Mukhanov, Ferromagnetic Josephson switching device with high characteristic voltage. *Appl. Phys. Lett.* **100**, 222601 (2012)
15. V.V. Ryazanov, V.V. Bol'ginov, D.S. Sobanin, I.V. Vernik, S.K. Tolpygo, A.M. Kadin, O.A. Mukhanov, Magnetic Josephson junction technology for digital and memory applications. *Phys. Proc.* **36**, 35 (2012)
16. I.V. Vernik, V.V. Bol'ginov, S.V. Bakurskiy, A.A. Golubov, M.Y. Kupriyanov, V.V. Ryazanov, O.A. Mukhanov, Magnetic Josephson junctions with superconducting interlayer for cryogenic memory. *IEEE Trans. Appl. Supercond.* **23**, 1701208 (2013)
17. S.V. Bakurskiy, N.V. Klenov, I.I. Soloviev, V.V. Bol'ginov, V.V. Ryazanov, I.V. Vernik, O.A. Mukhanov, M.Y. Kupriyanov, A.A. Golubov, Theoretical model of superconducting spintronic SISFS devices. *Appl. Phys. Lett.* **102**, 192603 (2013)
18. A.I. Buzdin, Proximity effects in superconductor-ferromagnet heterostructures. *Rev. Mod. Phys.* **77**, 935 (2005)
19. V.V. Ryazanov, V.A. Oboznov, A.Y. Rusanov, A.V. Veretennikov, A.A. Golubov, J. Aarts, Coupling of two superconductors through a ferromagnet: evidence of a pi-junction. *Phys. Rev. Lett.* **86**, 2427 (2001)
20. V.A. Oboznov, V.V. Bol'ginov, A.K. Feofanov, V.V. Ryazanov, A.I. Buzdin, Thickness dependence of the Josephson ground states of superconductor–ferromagnet–superconductor junctions. *Phys. Rev. Lett.* **96**, 197003 (2006)
21. A.V. Shcherbakova, K.G. Fedorov, K.V. Shulga et al., Fabrication and measurements of hybrid Nb/Al Josephson junctions and flux qubits with pi-shifters. *Supercond. Sci. Technol.* **28**, 025009 (2015)
22. A.I. Buzdin, L.N. Bulaevskii, S.V. Panjukov, Critical-current oscillations as a function of the exchange field and thickness of the ferromagnetic metal (F) in an S–F–S Josephson junction. *JETP Lett.* **35**, 178 (1982)
23. A.I. Buzdin, B. Bujicic, M.Y. Kupriyanov, Superconductor–ferromagnet structures. *Sov. Phys. JETP* **74**, 124 (1992)

24. L.N. Bulaevskii, V.V. Kuzii, A.A. Sobyenin, Superconducting system with weak coupling to the current in the ground state. *Pis'ma Zh. Eksp. Theor. Phys.* **25**, 314. *JETP Lett.* **25**, 290 (1977)
25. I.S. Veshchunov, V.A. Oboznov, A.N. Rossolenko, A.S. Prokofiev, L.Y. Vinnikov, A.Y. Rusanov, D.V. Matveev, Observation of the magnetic domain structure in CuNi thin films at low temperatures. *JETP Lett.* **88** 758. [*Pis'ma v ZHETF* 88, 873] (2008)
26. V.I. Zdravkov, J. Kehrle, G. Obermeier et al., Experimental observation of the triplet spin-valve effect in a superconductor-ferromagnet heterostructure. *Phys. Rev. B* **87**, 144507 (2013)
27. B. Baek, W.H. Rippard, S.P. Benz, S.E. Russek, P.D. Dresselhaus, Hybrid superconducting-magnetic memory device using competing order parameters. *Nat. Commun.* **5**, 3888 (2014)
28. E.C. Gingrich, B.M. Niedzielski, J.A. Glick, Y. Wang, D.L. Miller, R. Loloee, W.P. Pratt Jr., N.O. Birge, Controllable $0-\pi$ Josephson junctions containing a ferromagnetic spin valve. *Nat. Phys.* **12**, 564 (2016)
29. V.V. Ryazanov, V.A. Oboznov, A.V. Veretennikov et al., Intrinsically frustrated superconducting array of superconductor-ferromagnet-superconductor π junctions. *Phys. Rev. B* **65**, 020501 (2002)
30. R.G. Chambers, The anomalous skin effect. *Proc. R. Soc.* **215**, 481 (1952)
31. M. Gurvitch, M.A. Washington, H.A. Huggins, High quality refractory Josephson tunnel junctions utilizing thin aluminum layers. *Appl. Phys. Lett.* **42**, 472 (1983). <https://doi.org/10.1063/1.93974>
32. T. Kontos, M. Aprili, J. Lesueur et al., Josephson junction through a thin ferromagnetic layer: negative coupling. *Phys. Rev. Lett.* **89**, 137007 (2002)
33. H. Sellier, C. Baraduc, F. Lefloch, R. Calemczuk, Temperature-induced crossover between 0 and π states in S-F-S junctions. *Phys. Rev. B* **68**, 054531 (2003)
34. C. Bell, G. Burnell, D.-J. Kang, R.H. Hadfield, M.J. Kappers, M.G. Blamire, Fabrication of nanoscale heterostructure devices with a focused ion beam microscope. *Nanotechnology* **14**, 630 (2003)
35. J.W.A. Robinson, S. Piano, G. Burnell, C. Bell, M.G. Blamire, Critical current oscillations in strong ferromagnetic π -junctions. *Phys. Rev. Lett.* **97**, 177003 (2006)
36. M. Weides, E. Goldobin, D. Koelle, R. Kleiner, H. Kohlstedt, A. Buzdin, High quality ferromagnetic 0 and π Josephson tunnel junctions. *Appl. Phys. Lett.* **89**, 122511 (2006)
37. T.S. Khaire, W.P. Pratt Jr., N.O. Birge, Critical current behavior in Josephson junctions with the weak ferromagnet PdNi. *Phys. Rev. B* **79**, 094523 (2009)
38. M.Y. Kupriyanov, V.F. Lukichev, Influence of boundary transparency on the critical current of "dirty" SS'S structures. *Zh. Eksp. Teor. Fiz.* **94**, 139. *Sov. Phys. JETP* **67**, 1163 (1988)
39. A.A. Bannykh, J. Pfeiffer, V.S. Stolyarov, I.E. Batov, V.V. Ryazanov, M. Weides, Josephson tunnel junctions with a strong ferromagnetic interlayer. *Phys. Rev. B* **79**, 054501 (2009)
40. S.M. Frolov, D.J. Van Harlingen, V.V. Bolginov, V.A. Oboznov, V.V. Ryazanov, Josephson interferometry and Shapiro step measurements of superconductor-ferromagnet-superconductor $0-\pi$ junctions. *Phys. Rev. B* **74**, 020503(R) (2006)
41. Z. Radovic, L. Dobrosavljevic-Grujic, B. Vujicic, Coexistence of stable and metastable 0 and π states in Josephson junctions. *Phys. Rev. B* **63**, 214512 (2001)
42. A. Buzdin, Peculiar properties of the Josephson junction at the transition from 0 to π state. *Phys. Rev. B* **72**, 100501 (2005)